Noninvasive machine-learning models for the detection of lesion-specific ischemia in patients with stable angina with intermediate stenosis severity on coronary CT angiography

Hiroshi Hamasaki, RT[1,2], Hidetaka Arimura, PhD[3], Yuzo Yamasaki, MD, PhD[4], Takayuki Yamamoto, MS[2], Mitsuhiro Fukata, MD, PhD[5], Tetsuya Matoba, MD, PhD[6], Toyoyuki Kato, RT[2], Kousei Ishigami, MD, PhD [4]

Division of Medical Quantum Science, Department of Health Sciences, [1]Graduate School of Medical Sciences and [3]Faculty of Medical Sciences, Kyushu University, 3-1-1, Maidashi, Higashi-ku, Fukuoka 812-8582, Japan

[2]Division of Radiology, Department of Medical Technology, Kyushu University Hospital, 3-1-1, Maidashi, Higashi-ku, Fukuoka 812-8582, Japan

Department of [4]Clinical Radiology and [6]Cardiovascular Medicine, Graduate School of Medical Sciences, Kyushu University, 3-1-1, Maidashi, Higashi-ku, Fukuoka 812-8582, Japan

[5]Department of Hematology, Oncology and Cardiovascular Medicine, Kyushu University Hospital, 3-1-1, Maidashi, Higashi-ku, Fukuoka 812-8582, Japan

For corresponding authors

Hidetaka Arimura, PhD

Division of Medical Quantum Science, Department of Health Sciences, Faculty of Medical Sciences, Kyushu University

3-1-1, Maidashi, Higashi-ku, Fukuoka 812-8582, Japan

Tel/Fax: +81-(92)-642-6719

Email: arimura.hidetaka.616@m.kyushu-u.ac.jp

Yuzo Yamasaki, MD, PhD

Department of Clinical Radiology, Graduate School of Medical Sciences, Kyushu University, 3-1-1, Maidashi, Higashi-ku, Fukuoka 812-8582, Japan

Tell: +81-(92)-642-5695

Email: yamasaki.yuzo.776@m.kyushu-u.ac.jp

Abstract

This study proposed noninvasive machine-learning models for the detection of lesion-specific ischemia (LSI) in patients with stable angina with intermediate stenosis severity based on coronary computed tomography (CT) angiography. This single-center retrospective study analyzed 76 patients (99 vessels) with stable angina who underwent coronary CT angiography (CCTA) and had intermediate stenosis severity (40%-69%) on invasive coronary angiography. LSI, defined as a resting full-cycle ratio <0.86 or fractional flow reserve ≤0.80, was determined in 40 patients (46 vessels) using a hybrid resting full-cycle ratio-fractional flow reserve strategy. The resting full-cycle ratio and/or fractional flow reserve were measured using invasive coronary angiography as references for functional severity indices of coronary stenosis in the machine-learning models. LSI detection models were constructed using noninvasive machine-learning models that predicted the resting full-cycle ratio and fractional flow reserve by feeding machine-learning models with image features extracted from CCTA. The diagnostic performance of the proposed LSI detection models was assessed using a nested 10-fold cross-validation test. The LSI detection models with the highest diagnostic performance achieved an accuracy of 0.88 (95% CI: 0.81, 0.94), sensitivity of 0.78 (95% CI: 0.70, 0.86) and specificity of 0.96 (95% CI: 0.92, 1.00) on a vessel basis and 0.88 (95% CI: 0.81, 0.95), 0.80 (95% CI: 0.70, 0.86) and 0.97 (95% CI: 0.92, 1.00), respectively, on a patient basis. These findings suggest that LSI detection models with features extracted from CCTA can noninvasively detect LSI in patients with stable angina with intermediate stenosis severity.

Keywords

Noninvasive machine-learning models, Lesion-specific ischemia, Diameter stenosis severity, Hybrid resting full-cycle ratio and fractional flow reserve strategy

Acknowledgments

The authors are grateful to all members of the Arimura Laboratory (http://web.shs.kyushu-u.ac.jp/arimura) whose comments contributed to this study.

Declarations

Funding: This study was supported by the Bayer Research Grant Program of the Japan Radiological Society (KJ-2019-2).

Competing Interests: All authors declare no financial interests or personal relationships that could have influenced the work reported in this paper.

Ethical approval: This retrospective observational study was approved by the Institutional Review Board of Kyushu University Hospital, which waived the need for written informed consent.

Author contributions: Conceptualization: HH and HA. Data curation: HH, TY, TK, and HA. Formal analysis: HH, HA, YY, MF, TM, and KI. Funding acquisition: YY. Investigation: HH, HA, and TY. Methodology: HH, HA, and YY. Project administration: HA, YY, and KI. Resources: YY, MF, TM, TK, and KI. Software: HH, HA, and TY. Supervision: HA, YY, and KI. Validation: HH and HA. Visualization: HH, HA, and TY. Writing—original draft: HH, HA, and YY.

Introduction

Stable angina, an ischemic heart disease in which coronary artery stenosis results in reduced blood flow to the myocardium, remains the leading cause of death globally [1]. Treatment options for stable angina are selected according to the severity of coronary stenosis based on vessel diameter and/or functional severity indices based on pressure [2-5]. To detect lesion-specific ischemia (LSI) causing stable angina, the severity of coronary stenosis should first be evaluated using invasive coronary angiography (ICA) with catheters inserted through the coronary arteries. However, if patients have stable angina with intermediate stenosis severity (40%-69%) measured with ICA [6-8], functional severity indices of coronary stenosis, that is, the fractional flow reserve (FFR) and resting full-cycle ratio (RFR), are measured after ICA to determine the presence of LSI [4].

The standard FFR is obtained from the ICA as the ratio of coronary pressure (Pd) to aortic pressure (Pa) distal to the stenosis, using a pressure-measuring guidewire during maximum hyperemia using vasodilators [9]. However, the standard FFR remains underutilized due to its time and cost, as well as associated side effects (chest discomfort linked to the use of certain vasodilators) [10]. Recently, a new invasive approach to measure FFR without using pressure wires and induction of maximal hyperemia on the ICA [FFRangio system (CathWorks, Kfar Saba, Israel)] has become available by adapting rapid flow analysis (RFA) [11-13]. However, the FFRangio system remains invasive because ICA image acquisition is required, and the accuracy of FFRangio is lower than that of the standard FFR. RFR, which is defined on ICA as the minimum value of Pd/Pa within the entire cardiac cycle, can be used to detect LSI without inducing maximum hyperemia [14, 15]. RFR is increasingly used because it can significantly reduce the incidence of vasodilator-related side effects; however, it is not as accurate as FFR in assessing functional severity [16]. To overcome this issue, an invasive hybrid strategy using both the RFR and FFR has been proposed, which can reduce the use of vasodilators while maintaining a high classification agreement rate (95%) compared to FFR alone [3]. However, measurements of RFR and FFR using ICA can cause major cardiovascular complications or even death, as in the worst case [17-20]. Therefore, noninvasive predictions of RFR and FFR without ICA are desired for the detection of LSI in patients with stable angina and intermediate stenosis severity.

Two types of noninvasive approaches, computational fluid dynamics (CFD) and machine-learning (ML),

have been investigated. Early studies on CFD-based approaches demonstrated that computer-based techniques could detect LSI [21-24], but the long computational time required might render the techniques clinically infeasible. Furthermore, the accuracies of LSI detection of CFD-based approaches were lower than 0.5 for predicted FFRs in the range of 0.70-0.80 [22, 24]. On the other hand, several ML-based approaches have attempted to reduce the computational costs [25-27]. However, no previous study has investigated noninvasive approaches for the detection of LSI based on RFR and FFR simultaneously predicted with ML. Approaches with higher specificity and positive predictive values (PPVs) are needed for definitive diagnosis with fewer false positives, thereby avoiding unnecessary tests. However, previous studies did not demonstrate improvements in the specificities and PPVs of LSI detection for predicted FFRs in the range of 0.70-0.80.

We hypothesized that the prediction of RFR and FFR using ML models would allow the noninvasive detection of LSI with higher specificities and PPVs. ML models should be fed with image features obtained from noninvasive coronary computed tomography angiography (CCTA) with intravenous infusion of contrast media without using catheters. CCTA has a low risk of serious complications [28, 29]. The purpose of this study was to propose noninvasive ML models for LSI detection (hereafter, LSI detection models) that can predict functional severity indices (RFR and FFR) on CCTA. To demonstrate the feasibility of the proposed LSI detection models, we focused exclusively on patients with intermediate stenosis severity.

Methods

Patient data

This retrospective observational study was approved by the institutional review board of our hospital, which waived the need for written informed consent. This study enrolled 88 patients with stable angina who underwent CCTA from September 2019 to May 2021, followed by the measurement of RFR and FFR on the ICA within 60 days, and had intermediate stenosis severity on the ICA. Intermediate ICA-based stenosis severity was defined as a lumen diameter between 40% and 69% [4] of the maximum stenotic section relative to the nonstenotic section. The need for ICA was decided based on clinical presentations, CCTA imaging findings, and results of noninvasive functional tests [30]. The exclusion criteria were low-quality CCTA images, prior myocardial infarction, and

previous coronary artery bypass grafting. Among the 88 patients, 12 were excluded, including 8 patients with low-quality CCTA images, 2 patients with previous coronary artery bypass graft, and 2 patients with inappropriate RFR measurements. Thus, a total of 76 patients were included in the analysis.

CCTA images of all the patients were acquired using a 320-slice computed tomography (CT) scanner (Aquilion Prime; Canon Medical Systems, Otawara, Japan). Prior to CCTA scanning, a sublingual nitroglycerin spray was administered to all patients. CCTA scans were triggered using an automatic bolus-tracking technique, with the region of interest placed in the ascending thoracic aorta. Both prospective triggering and retrospective gating were used for the CCTA acquisition. CCTA scan parameters were as follows: gantry rotation time, 0.275 s; tube voltage, 120 or 100 kV; matrix size, 512 × 512; in-plane pixel size, 0.35 or 0.31 mm; slice thickness, 0.5 mm; and section interval, 0.25 mm. The CCTA dataset was anonymized, and the CCTA-based stenosis severity was evaluated by a cardiac radiologist (Y.Y.) with 15-years' experience. CCTA-based stenosis severity for all coronary segments ≥2 mm in maximum diameter was classified according to the guidelines [31].

ICA images were acquired using a standard protocol in at least two orthogonal directions per evaluated coronary artery segment. After visual assessment of the coronary lesions on the ICA, invasive RFR and/or FFR were additionally measured using a PressureWire™ X Guidewire 0.014 (Abbott Vascular Inc., Santa Clara, CA, USA) positioned far distal to the lesion with an intermediate ICA-based stenosis severity. To measure FFR, maximum hyperemia was induced using intravenous adenosine (140 μg/kg/min). Figure 1 shows the flowchart of LSI detection based on the hybrid RFR-FFR strategy [3, 32] used in this study. In this study, RFRs were measured in vessels with an intermediate ICA-based stenosis severity. Vessels with RFR >0.93 were regarded as non-LSI, while vessels with RFR <0.86 were regarded as LSI. For cases with an intermediate RFR (0.86 to 0.93), the FFR was additionally measured to reclassify the vessels. Finally, vessels with FFR ≤0.80 were regarded as LSI, while vessels with FFR >0.80 were regarded as non-LSI. RFR was measured in 76 patients (99 vessels) and FFR was obtained in 64 patients (78 vessels).

Overall scheme for developing noninvasive LSI detection models

Figure 2 illustrates the overall workflow of the proposed approach for noninvasive LSI detection. Forty-two

noninvasive features were extracted from the CCTA images and clinical information. Among these, the significant features for predicting the RFR and FFR were determined separately using 5 feature selection methods. RFR and FFR prediction models were built using 10 regression algorithms with significant features. LSI detection models were constructed by incorporating RFR and FFR prediction models into the hybrid RFR-FFR strategy. Finally, the LSI detection models were evaluated for accuracy, sensitivity, specificity, PPV, and negative predictive value (NPV). The model with the highest accuracy for predicted FFRs in the range of 0.70 to 0.80 was considered as the best LSI detection model.

Feature extraction

A total of 42 noninvasive features were extracted from the CCTA images and clinical information. The definitions of the features used in the prediction models are summarized in Table 1. Twenty-seven features were independently and randomly measured on CCTA using a 3-dimensional image analysis system (Synapse Vincent; Fujifilm, Tokyo, Japan) based on the consensus of two radiological technologists (H.H. and T.Y., with 10 and 3 years of experience in cardiac CT, respectively) and a cardiac radiologist (Y.Y., with 15 years of experience). The observers were blinded to the patients' histories and the ICA results. All discordant cases (n=4) were re-evaluated for consensus interpretation. In cases with multiple lesions in a vessel, features were extracted for each lesion.

The following features related to coronary artery stenosis were extracted: the difference and differential ratio in CT values between nonstenotic and stenotic sections and lesion length (Fig. 2). CT values for nonstenotic (CTn) and stenotic sections (CTs) of the coronary artery were measured using cross-sectional images. The CTn value was defined as the mean CT value of nonstenotic sections proximal and distal to the stenosis, while the CTs value was defined as the mean CT value of the section with CCTA-based stenosis severity ≥25%. The difference and differential ratio of CT values between CTn and CTs (defined as the ratio of CTn minus CTs to CTn) were determined. The lesion length was measured on stretched curved multiplanar reconstruction images as the length of the section with a CCTA-based stenosis severity ≥25%. CCTA-derived myocardial mass (CMM) perfused into each coronary artery was calculated using an algorithm based on Voronoi tessellation [33, 34]. CMMs were calculated at each of the two observer-specified points: at the origin of the main coronary artery, including the

target lesion, and at the end of the target lesion. A myocardial mass at risk was defined as a CMM when the end of the target lesion was indicated [35].

Additionally, 15 features were extracted from clinical information, including age, sex, and body mass index.

Feature selection

Among the extracted 42 features, significant features in the prediction models were selected using 5 feature-selection methods. The significant features were ranked based on the product of the selected frequencies and coefficients. The best features are those used in the best LSI detection model. Among the 5 feature selection methods, three are wrapper methods (recursive feature elimination, sequential forward floating selection, and sequential backward floating selection) and two are embedded methods (elastic net and extreme gradient boosting). For each feature selection method, the RFR and FFR prediction models were adjusted to select no more than 7 and 6 features, respectively. This is in accordance with the rule of thumb that the largest number of features must be less than or equal to one-tenth of the number of cases (i.e., the largest number of features: round [76/10] = 7 for RFR and round [64/10] = 6 for FFR) [36, 37].

RFR and FFR prediction model construction

RFR and FFR prediction models were constructed independently using 10 different regression algorithms: support vector regression (SVR), least absolute shrinkage and selection operator, ridge, elastic net, partial least squares (PLS), k-nearest neighbor, multilayer perceptron, random forest, extreme gradient boosting, and light gradient boosting. For each regression algorithm adapted to the significant features, the optimal prediction model was identified by performing a nested 10-fold cross-validation. The optimal prediction model was adjusted to minimize the root mean square error between the training and validation datasets. The predicted RFR and FFR were set to 1.0 if they exceeded 1.0. Eighty-eight prediction models (Table 2) were built from a combination of 5 feature selection methods and 10 regression algorithms to find an optimal prediction model for the RFR and FFR.

Construction and evaluation of LSI detection models

A total of 7744 LSI detection models were constructed by incorporating 88 RFR and FFR prediction models into the hybrid RFR-FFR strategy (Fig. 1). All models were implemented using Python [version 3.11]. LSI detection models were tested on all vessels in the dataset using a nested 10-fold cross-validation test [38]. The advantage of the nested 10-fold cross-validation test is that the models can be trained using validation tests in the inner loop and an independent test in the outer loop. These noninvasive LSI detection models were evaluated with reference to the invasive hybrid RFR-FFR strategy according to their accuracy, sensitivity, specificity, PPV, and NPV for detecting LSI.

Statistical analysis

All statistical analyses were performed using JMP Pro version 16.2.0 (SAS Institute Inc., Cary, NC, United States). Continuous variables are presented as mean ± standard deviation or median, as appropriate. Categorical variables were expressed as frequencies and percentages. Differences in continuous baseline characteristic variables between the LSI and non-LSI cohorts were compared using the two-tailed Student t-test; differences in categorical baseline variables were analyzed using the chi-square test or Fisher's exact test, as appropriate. Correlations between the predicted and measured values of the functional severity indices were analyzed using Pearson's correlation coefficient. The degree of agreement between the predicted and measured values of the functional severity indices was assessed using Bland-Altman analysis. The limits of agreement in the analysis were defined as the mean difference ± 1.96 × the standard deviation of the differences, and systematic biases in the differences between the predicted and measured values were evaluated. Patients with LSI in at least one vessel were considered to be positive for LSI. Accuracy, sensitivity, specificity, PPV, and NPV were reported with corresponding 95% confidence intervals. A *P*-value <.05 was considered statistically significant.

Results

A total of 76 patients (99 vessels) were evaluated using an invasive hybrid RFR-FFR strategy; 40 patients (46 vessels) were classified as LSI (mean age, 74 ± 12 [standard deviation] years; 26 men) and 36 patients (53 vessels)

were classified as non-LSI (mean age, 70 ± 12 years; 25 men). The patient demographics are summarized in Table 3.

The combined ridge plus SVR (ridge-SVR) and PLS plus ridge (PLS-ridge) models achieved the highest diagnostic performance for noninvasively detecting LSI among the 7744 prediction models; Table 4 lists the top 5 features used in the 10 subsets of these models. The top-ranked features used in the RFR and FFR prediction models were extracted from the CCTA images. In the RFR prediction model, the differential ratio of CT values and myocardial mass at risk were the most significant features. In addition, the difference in CT values, product of the differential ratio in CT values and lesion length, and CMM in the major coronary artery containing the lesion were significant features in the FFR prediction model. Scatter plots of the top features of the ridge-SVR model are shown in Figure 3.

Table 5 shows the diagnostic performances of the ridge-SVR and PLS-ridge models on vessel and patient bases. On a vessel basis, the ridge-SVR and PLS-ridge models exhibited the same accuracy (0.88, 87/99). The PLS-ridge model achieved the highest sensitivity (0.83; 38/46), whereas the ridge-SVR model achieved the highest specificity (0.96; 51/53). The ridge-SVR and PLS-ridge models exhibited root-mean-square errors of 0.083 and 0.081, respectively. On a patient basis, the ridge-SVR and PLS-ridge models showed comparable accuracies (0.88 and 0.87, 67/76, and 66/76, respectively). Furthermore, the PLS-ridge model achieved the highest sensitivity (0.85; 34/40), whereas the ridge-SVR model achieved the highest specificity (0.97; 35/36). For vessels with a predicted FFR in the range of 0.70 to 0.80, the ridge-SVR model achieved the highest accuracy (0.89, 17/19) and was considered the best LSI detection model. Previous studies on LSI detection based on invasive and noninvasive approaches are summarized in Table 6. The proposed noninvasive approach had the highest specificity (0.96). Representative patients with LSI and non-LSI based on invasive FFR measurements are shown in Figure 4. In the first patient (Fig. 4a and b), invasive and predicted FFRs were both 0.75 for the lesion, and the LSI was accurately detected. In the second patient (Fig. 4c and d), the invasive and predicted FFRs were both 0.81 for the lesion, which was determined to be non-LSI.

Figures 5 and 6 show the results of the evaluation of the predicted RFRs and FFRs, respectively, by Pearson correlation and Bland-Altman analyses. The correlation coefficient between invasive RFR and RFR in the

ridge prediction model indicated a moderate positive correlation (r=0.46, P<.001) (Fig. 5a). In the Bland-Altman analysis (Fig. 5b), the mean difference between the RFR in the ridge prediction model and the invasive RFR was 0.002, and most of the data were distributed within the limits of agreement (-0.15 to 0.15). The correlation coefficient between the FFR in the SVR prediction model and invasive FFR indicated a moderate positive correlation (r=0.55, P<.001) (Fig. 6a). The results for the FFR SVR prediction model were similar to those for the RFR ridge prediction model, with a mean difference value of -0.0007 and limits of agreement ranging from -0.15 to 0.15 (Fig. 6b).

Discussion

We found that our prediction model for noninvasive LSI detection performed well by utilizing the features extracted from CCTA images and clinical information of 76 patients with stable angina. The ridge-SVR model, which achieved the highest accuracy of 0.89 for predicted FFRs in the range of 0.70 to 0.80, was considered to be the best model for noninvasive detection of LSI. Furthermore, the ridge-SVR model showed the highest accuracies of 0.88 for vessels and 0.88 for patients and highest specificity of 0.96 for vessels and 0.97 for patients. The significant features utilized in the ridge-SVR model, including the difference and differential ratio in CT values, along with the myocardial mass, were extracted from the noninvasive CCTA images.

The accuracy of LSI detection close to the FFR threshold of 0.80 is crucial for guiding appropriate treatments for stable angina. In the present study, the accuracy of LSI detection reached 0.89 in the range of predicted FFRs of 0.70 to 0.80, indicating a substantial improvement compared to those of 0.46 and 0.32 in CFD-based studies by Cook et al. [22] and Matsumura-Nakano et al. [24]. This improvement may be attributed to small variations in the invasive FFR of training data. Specifically, 28% (22/78) of patients in this study were in the range of invasive FFR of 0.70 to 0.80, compared with 13% in the study of Cook et al. [22]. Furthermore, 53/78 (68%) vessels presented with lesions proximate to the FFR threshold (0.70-0.90). The limited range of invasive FFR in our study resulted from targeting lesions with intermediate ICA-based stenosis severity and employing a hybrid RFR-FFR strategy. In addition, ML-based methods offer a distinct advantage over CFD-based methods owing to their significantly shorter computation times [25, 26].

The proposed approach can predict RFRs and FFRs simultaneously and reveal significant features that contribute to their prediction. Three types of conventional approaches (RFA, CFD, and ML) for FFR prediction provided predicted FFRs without disclosing significant features. In this study, the best features for predicting RFR and FFR were the difference and difference ratio in CT values, as well as the myocardial mass on CCTA (Table 4). Previous studies have shown that these features are beneficial for LSI detection [33, 39, 40]. Thus, features extracted from CCTA images could be used for noninvasive measurements of RFR and FFR using ML. Furthermore, it is possible to predict post-revascularization RFR and FFR by identifying the significant features that contribute to the prediction of RFR and FFR. Therefore, the clinical applicability of these models can be expanded.

The proposed ML-based models for the prediction of the RFR and FFR yielded the highest specificity and PPV among previous studies on LSI detection approaches (Table 6). The specificity of the proposed ML model was superior to those of the CFD-based (0.93) and ML-based models (0.94) in the study by Tesche et al. [25]. This may be because RFR and FFR were simultaneously predicted using ML for the detection of LSI. In contrast, previous studies based on RFA, CFD, and ML reported higher sensitivities for LSI detection (0.81-0.91) [13, 23, 26] than that in the present study (0.78). Our study targeted patients exhibiting intermediate ICA-based stenosis severity (40%-69%), while previous studies included apparent LSI cases (≥70% ICA-based stenosis severity). As the target population has a significant impact on the diagnostic performance, we could develop an LSI detection system for all stenosis severities in future studies.

CCTA-based stenosis severity assessment has proven to be more sensitive and offers a higher NPV than current noninvasive functional testing methods, which helps reduce the number of non-LSI patients during ICA [41, 42]. The proposed ML-based models can accurately exclude lesions with an invasive FFR >0.80 and CCTA-based stenosis severity ≥50% from the LSI, allowing non-invasive anatomic and physiologic assessment of stable angina. An effective diagnostic process can be established in which the proposed models can be applied after CCTA-based stenosis severity assessment without additional testing or exposure to radiation or contrast agents [43, 44]. In addition, the proposed models may simplify LSI detection testing and increase diagnostic accuracy, thereby improving the quality of patient care and promoting the efficient use of healthcare resources [45]. As a

result, healthcare costs are reduced and patients are more receptive to testing, making early diagnosis and treatment more feasible [46]. However, further investigation is necessary to fully explore the potential of these advantages.

The present study had some limitations. First, this was a single-center, retrospective study involving a relatively small cohort of patients. Therefore, it was validated using a nested 10-fold cross-validation test but lacked an external test cohort from different institutions. A larger study is required to validate our findings and to provide more representative results. Second, we did not measure coronary artery calcium scores. This is because we did not perform non-enhanced CT imaging for calcium scoring during the CCTA examinations at our institution. High calcium scores prevent the accurate measurement of CT values, which was considered a useful feature in this study, and could have affected the diagnostic performance of the LSI detection models. Third, most feature extractions from the CCTA images were performed manually. Although the features were measured by two radiological technologists to reduce uncertainty and subjective bias, automated methods are necessary to improve the reproducibility and objectivity. Fourth, this study included patients with stable angina and excluded those with acute coronary syndrome or history of coronary artery bypass grafting. Therefore, the generalizability of our LSI detection models to patients with ischemic heart disease is uncertain.

Conclusions

We proposed noninvasive LSI detection models based on the prediction of RFR and FFR using CCTA. The results of this study demonstrate that the proposed model using CCTA could be feasible for noninvasive LSI detection in patients with stable angina and intermediate stenosis severity. The LSI detection model employing ridge-SVR was found to be the most effective, achieving an accuracy of 0.88, sensitivity of 0.78, and specificity of 0.96 on a vessel basis and 0.88, 0.80, and 0.97, respectively, on a patient basis. Furthermore, the significant features extracted from CCTA demonstrated the ability to predict both the RFR and FFR.

References

[1] World Health Organization (2020) WHO reveals leading causes of death and disability worldwide: 2000–2019. WHO Publishing. http://www.who.int/news/item/09-12-2020-who-reveals-leading-causes-of-death-and-disability-worldwide-2000-2019. Accessed 19 November 2023

[2] Knuuti J, Wijns W, Saraste A, Capodanno D, Barbato E, Funck-Brentano C, et al. (2020) 2019 ESC Guidelines for the diagnosis and management of chronic coronary syndromes: the Task Force for the diagnosis and management of chronic coronary syndromes of the European Society of Cardiology (ESC). Eur Heart J 41:407-477. https://doi.org/10.1093/eurheartj/ehz425

[3] Casanova-Sandoval J, Fernandez-Rodriguez D, Otaegui I, Gil Jimenez T, Rodriguez-Esteban M, Rivera K, et al. (2021) Usefulness of the Hybrid RFR-FFR Approach: Results of a Prospective and Multicenter Analysis of Diagnostic Agreement between RFR and FFR-The RECOPA (REsting Full-Cycle Ratio Comparation versus Fractional Flow Reserve (A Prospective Validation)) Study. J Interv Cardiol 2021:5522707. https://doi.org/10.1155/2021/5522707

[4] Lawton JS, Tamis-Holland JE, Bangalore S, Bates ER, Beckie TM, Bischoff JM, et al. (2022) 2021 ACC/AHA/SCAI Guideline for coronary artery revascularization: A report of the american college of cardiology/american heart association joint committee on clinical practice guidelines. J Am Coll Cardiol 79:e21-e129. https://doi.org/10.1016/j.jacc.2021.09.006

[5] Gould KL, Lipscomb K, Hamilton GW (1974) Physiologic basis for assessing critical coronary stenosis: Instantaneous flow response and regional distribution during coronary hyperemia as measures of coronary flow reserve. Am J Cardiol 33:87–94. https://doi.org/10.1016/0002-9149(74)90743-7

[6] Fischer JJ, Samady H, McPherson JA, Sarembock IJ, Powers ER, Gimple LW, et al. (2002) Comparison between visual assessment and quantitative angiography versus fractional flow reserve for native coronary narrowings of moderate severity. The American journal of cardiology 90:210-215. https://doi.org/10.1016/S0002-9149(02)02456-6

[7] Meijboom WB, Van Mieghem CA, van Pelt N, Weustink A, Pugliese F, Mollet NR, et al. (2008) Comprehensive assessment of coronary artery stenoses: computed tomography coronary angiography versus

conventional coronary angiography and correlation with fractional flow reserve in patients with stable angina. J Am Coll Cardiol 52:636-643. https://doi.org/10.1016/j.jacc.2008.05.024

[8] Tonino PA, Fearon WF, De Bruyne B, Oldroyd KG, Leesar MA, Ver Lee PN, et al. (2010) Angiographic versus functional severity of coronary artery stenoses in the FAME study fractional flow reserve versus angiography in multivessel evaluation. J Am Coll Cardiol 55:2816-2821. https://doi.org/10.1016/j.jacc.2009.11.096

[9] Pijls NHJ, DeBruyne B, Peels K, VanderVoort PH, Bonnier HJRM, Bartunek J, et al. (1996) Measurement of Fractional Flow Reserve to Assess the Functional Severity of Coronary-Artery Stenoses. N Engl J Med 334:1703-1708. https://doi.org/10.1056/Nejm199606273342604

[10] Davies JE, Sen S, Dehbi HM, Al-Lamee R, Petraco R, Nijjer SS, et al. (2017) Use of the Instantaneous Wave-free Ratio or Fractional Flow Reserve in PCI. N Engl J Med 376:1824-1834. https://doi.org/10.1056/NEJMoa1700445

[11] Pellicano M, Lavi I, De Bruyne B, Vaknin-Assa H, Assali A, Valtzer O, et al. (2017) Validation Study of Image-Based Fractional Flow Reserve During Coronary Angiography. Circ Cardiovasc Interv 10. https://doi.org/10.1161/CIRCINTERVENTIONS.116.005259

[12] Fearon WF, Achenbach S, Engstrom T, Assali A, Shlofmitz R, Jeremias A, et al. (2019) Accuracy of Fractional Flow Reserve Derived From Coronary Angiography. Circulation 139:477-484. https://doi.org/10.1161/CIRCULATIONAHA.118.037350

[13] Witberg G, De Bruyne B, Fearon WF, Achenbach S, Engstrom T, Matsuo H, et al. (2020) Diagnostic Performance of Angiogram-Derived Fractional Flow Reserve: A Pooled Analysis of 5 Prospective Cohort Studies. JACC Cardiovasc Interv 13:488-497. https://doi.org/10.1016/j.jcin.2019.10.045

[14] Kumar G, Desai R, Gore A, Rahim H, Maehara A, Matsumura M, et al. (2020) Real world validation of the nonhyperemic index of coronary artery stenosis severity-Resting full-cycle ratio-RE-VALIDATE. Catheter Cardiovasc Interv 96:E53-E58. https://doi.org/10.1002/ccd.28523

[15] Lee JM, Choi KH, Park J, Hwang D, Rhee TM, Kim J, et al. (2019) Physiological and Clinical Assessment of Resting Physiological Indexes. Circulation 139:889-900. https://doi.org/10.1161/CIRCULATIONAHA.118.037021

[16] Svanerud J, Ahn JM, Jeremias A, van 't Veer M, Gore A, Maehara A, et al. (2018) Validation of a novel non-hyperaemic index of coronary artery stenosis severity: the Resting Full-cycle Ratio (VALIDATE RFR) study. EuroIntervention 14:806-814. https://doi.org/10.4244/EIJ-D-18-00342

[17] Jr. TJN, Johnson LW, Krone R, Weaver WF, Clark DA, Jr. JRK, et al. (1991) Cardiac catheterization 1990: A report of the registry of the society for cardiac angiography and interventions (SCAI). Cathet Cardiovasc Diagn 24:75-83.

[18] Lund C, Nes RB, Ugelstad TP, Due-Tonnessen P, Andersen R, Hol PK, et al. (2005) Cerebral emboli during left heart catheterization may cause acute brain injury. Eur Heart J 26:1269-1275. https://doi.org/10.1093/eurheartj/ehi148

[19] Jolly SS, Amlani S, Hamon M, Yusuf S, Mehta SR (2009) Radial versus femoral access for coronary angiography or intervention and the impact on major bleeding and ischemic events: a systematic review and meta-analysis of randomized trials. Am Heart J 157:132-140. https://doi.org/10.1016/j.ahj.2008.08.023

[20] Surhonne PS, Mahla H, Bhairappa S, Somanna S, Manjunath CN (2015) Successful retrieval of fractured pressure wire tip (FFR) by hybrid technique. J Saudi Heart Assoc 27:118-122. https://doi.org/10.1016/j.jsha.2014.09.001

[21] Taylor CA, Fonte TA, Min JK (2013) Computational fluid dynamics applied to cardiac computed tomography for noninvasive quantification of fractional flow reserve: scientific basis. J Am Coll Cardiol 61:2233-2241. https://doi.org/10.1016/j.jacc.2012.11.083

[22] Cook CM, Petraco R, Shun-Shin MJ, Ahmad Y, Nijjer S, Al-Lamee R, et al. (2017) Diagnostic Accuracy of Computed Tomography-Derived Fractional Flow Reserve : A Systematic Review. JAMA Cardiol 2:803-810. https://doi.org/10.1001/jamacardio.2017.1314

[23] Driessen RS, Danad I, Stuijfzand WJ, Raijmakers PG, Schumacher SP, van Diemen PA, et al. (2019) Comparison of Coronary Computed Tomography Angiography, Fractional Flow Reserve, and Perfusion Imaging for Ischemia Diagnosis. J Am Coll Cardiol 73:161-173. https://doi.org/10.1016/j.jacc.2018.10.056

[24] Matsumura-Nakano Y, Kawaji T, Shiomi H, Kawai-Miyake K, Kataoka M, Koizumi K, et al. (2019) Optimal Cutoff Value of Fractional Flow Reserve Derived From Coronary Computed Tomography Angiography for Predicting Hemodynamically Significant Coronary Artery Disease. Circ Cardiovasc Imaging 12:e008905. https://doi.org/10.1161/CIRCIMAGING.119.008905

[25] Tesche C, De Cecco CN, Baumann S, Renker M, McLaurin TW, Duguay TM, et al. (2018) Coronary CT Angiography-derived Fractional Flow Reserve: Machine Learning Algorithm versus Computational Fluid Dynamics Modeling. Radiology 288:64-72. https://doi.org/10.1148/radiol.2018171291

[26] Coenen A, Kim YH, Kruk M, Tesche C, De Geer J, Kurata A, et al. (2018) Diagnostic Accuracy of a Machine-Learning Approach to Coronary Computed Tomographic Angiography-Based Fractional Flow Reserve: Result From the MACHINE Consortium. Circ Cardiovasc Imaging 11:e007217. https://doi.org/10.1161/CIRCIMAGING.117.007217

[27] Tang CX, Guo BJ, Schoepf JU, Bayer RR, 2nd, Liu CY, Qiao HY, et al. (2021) Feasibility and prognostic role of machine learning-based FFRCT in patients with stent implantation. Eur Radiol 31:6592-6604. https://doi.org/10.1007/s00330-021-07922-w

[28] Meijboom WB, Meijs MF, Schuijf JD, Cramer MJ, Mollet NR, van Mieghem CA, et al. (2008) Diagnostic accuracy of 64-slice computed tomography coronary angiography: a prospective, multicenter, multivendor study. *J Am Coll Cardiol* **52**:2135-2144. https://doi.org/10.1016/j.jacc.2008.08.058

[29] Corballis N, Tsampasian V, Merinopoulis I, Gunawardena T, Bhalraam U, Eccleshall S, et al. (2023) CT angiography compared to invasive angiography for stable coronary disease as predictors of major adverse cardiovascular events- A systematic review and meta-analysis. *Heart Lung* **57**:207-213. https://doi.org/10.1016/j.hrtlng.2022.09.018

[30] Montalescot G, Sechtem U, Achenbach S, Andreotti F, Arden C, Budaj A, et al. (2013) 2013 ESC guidelines on the management of stable coronary artery disease: the Task Force on the management of stable coronary artery disease of the European Society of Cardiology. Eur Heart J 34:2949-3003. https://doi.org/10.1093/eurheartj/eht296

[31] Leipsic J, Abbara S, Achenbach S, Cury R, Earls JP, Mancini GJ, et al. (2014) SCCT guidelines for the interpretation and reporting of coronary CT angiography: a report of the Society of Cardiovascular Computed Tomography Guidelines Committee. J Cardiovasc Comput Tomogr 8:342-358. https://doi.org/10.1016/j.jcct.2014.07.003

[32] Escaned J, Echavarria-Pinto M, Garcia-Garcia HM, van de Hoef TP, de Vries T, Kaul P, et al. (2015) Prospective Assessment of the Diagnostic Accuracy of Instantaneous Wave-Free Ratio to Assess Coronary Stenosis Relevance: Results of ADVISE II International, Multicenter Study (ADenosine Vasodilator Independent Stenosis Evaluation II). JACC Cardiovasc Interv 8:824-833. https://doi.org/10.1016/j.jcin.2015.01.029

[33] Sumitsuji S, Ide S, Siegrist PT, Salah Y, Yokoi K, Yoshida M, et al. (2016) Reproducibility and clinical potential of myocardial mass at risk calculated by a novel software utilizing cardiac computed tomography information. Cardiovasc Interv Ther 31:218-225. https://doi.org/10.1007/s12928-015-0370-0

[34] Ide S, Sumitsuji S, Yamaguchi O, Sakata Y (2017) Cardiac computed tomography-derived myocardial mass at risk using the Voronoi-based segmentation algorithm: A histological validation study. J Cardiovasc Comput Tomogr 11:179-182. https://doi.org/10.1016/j.jcct.2017.04.007

[35] Sadamatsu K, Nagaoka K, Koga Y, Kagiyama K, Muramatsu K, Hironaga K, et al. (2020) The Functional Severity Assessment of Coronary Stenosis Using Coronary Computed Tomography Angiography-Based Myocardial Mass at Risk and Minimal Lumen Diameter. Cardiovasc Ther 2020:6716130. https://doi.org/10.1155/2020/6716130

[36] Peduzzi P, Concato J, Kemper E, Holford TR, Feinstein AR (1996) A simulation study of the number of events per variable in logistic regression analysis. J Clin Epidemiol 49:1373-1379. https://doi.org/10.1016/S0895-4356(96)00236-3

[37] Arimura H, Soufi M, Ninomiya K, Kamezawa H, Yamada M (2018) Potentials of radiomics for cancer diagnosis and treatment in comparison with computer-aided diagnosis. Radiol Phys Technol 11:365-374. https://doi.org/10.1007/s12194-018-0486-x

[38] Ruschhaupt M, Huber W, Poustka A, Mansmann U (2004) A compendium to ensure computational reproducibility in high-dimensional classification tasks. Stat Appl Genet Mol Biol 3:Article37. https://doi.org/10.2202/1544-6115.1078

[39] Park SJ, Kang SJ, Ahn JM, Shim EB, Kim YT, Yun SC, et al. (2012) Visual-functional mismatch between coronary angiography and fractional flow reserve. JACC Cardiovasc Interv 5:1029-1036. https://doi.org/10.1016/j.jcin.2012.07.007

[40] Choi JH, Koo BK, Yoon YE, Min JK, Song YB, Hahn JY, et al. (2012) Diagnostic performance of intracoronary gradient-based methods by coronary computed tomography angiography for the evaluation of physiologically significant coronary artery stenoses: a validation study with fractional flow reserve. Eur Heart J Cardiovasc Imaging 13:1001-1007. https://doi.org/10.1093/ehjci/jes130

[41] Douglas PS, Hoffmann U, Patel MR, Mark DB, Al-Khalidi HR, Cavanaugh B, et al. (2015) Outcomes of anatomical versus functional testing for coronary artery disease. *N Engl J Med* **372**:1291-1300. https://doi.org/10.1056/NEJMoa1415516

[42] Investigators S-H, Newby DE, Adamson PD, Berry C, Boon NA, Dweck MR, et al. (2018) Coronary CT Angiography and 5-Year Risk of Myocardial Infarction. *N Engl J Med* **379**:924-933. https://doi.org/10.1056/NEJMoa1805971

[43] Einstein AJ (2008) Radiation risk from coronary artery disease imaging: how do different diagnostic tests compare? Heart 94:1519. https://doi.org/10.1136/hrt.2007.135731

[44] Coenen A, Rossi A, Lubbers MM, Kurata A, Kono AK, Chelu RG, et al. (2017) Integrating CT Myocardial Perfusion and CT-FFR in the Work-Up of Coronary Artery Disease. JACC Cardiovasc Imaging 10:760-770. https://doi.org/10.1016/j.jcmg.2016.09.028

[45] Lossnitzer D, Chandra L, Rutsch M, Becher T, Overhoff D, Janssen S, et al. (2020) Additional Value of Machine-Learning Computed Tomographic Angiography-Based Fractional Flow Reserve Compared to Standard

Computed Tomographic Angiography. *J Clin Med* **9**. https://doi.org/10.3390/jcm9030676

[46] Douglas PS, De Bruyne B, Pontone G, Patel MR, Norgaard BL, Byrne RA, et al. (2016) 1-Year Outcomes of FFRCT-Guided Care in Patients With Suspected Coronary Disease: The PLATFORM Study. J Am Coll Cardiol 68:435-445. https://doi.org/10.1016/j.jacc.2016.05.057

Statements and Declarations

Funding: This study was supported by the Bayer Research Grant Program of the Japan Radiological Society (KJ-2019-2).

Competing Interests: All authors declare no financial interests or personal relationships that could have influenced the work reported in this paper.

Author contributions: Conceptualization: HH and HA. Data curation: HH, TY, TK, and HA. Formal analysis: HH, HA, YY, MF, TM, and KI. Funding acquisition: YY. Investigation: HH, HA, and TY. Methodology: HH, HA, and YY. Project administration: HA, YY, and KI. Resources: YY, MF, TM, TK, and KI. Software: HH, HA, and TY. Supervision: HA, YY, and KI. Validation: HH and HA. Visualization: HH, HA, and TY. Writing—original draft: HH, HA, and YY.

Ethical approval: This retrospective observational study was approved by the Institutional Review Board of Kyushu University Hospital, which waived the need for written informed consent.

Figure legends

Fig. 1 Flowchart for lesion-specific ischemia (LSI) detection based on the hybrid RFR-FFR strategy. RFR = resting full-cycle ratio; FFR = fractional flow reserve.

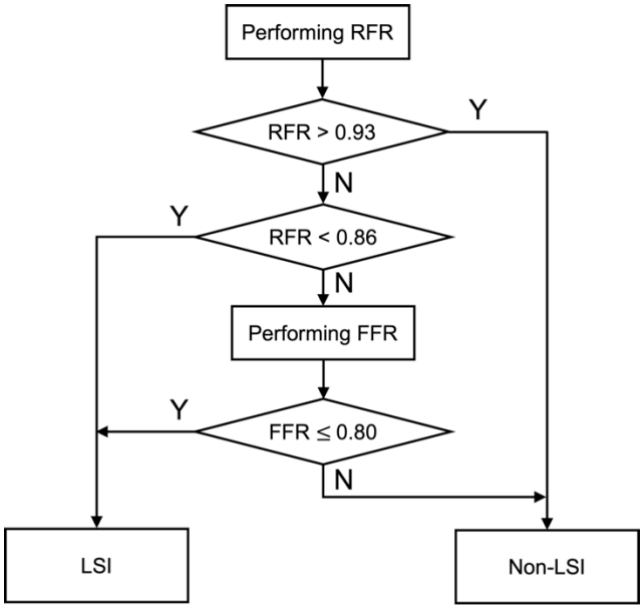

Fig. 2 Overall workflow for developing noninvasive LSI detection models. LSI = lesion-specific ischemia, CCTA = coronary computed tomography angiography, RFR = resting full-cycle ratio, FFR = fractional flow reserve, TP = true positive, TN = true negative, FN = false negative, FP = false positive, PPV = positive predictive value, NPV = negative predictive value.

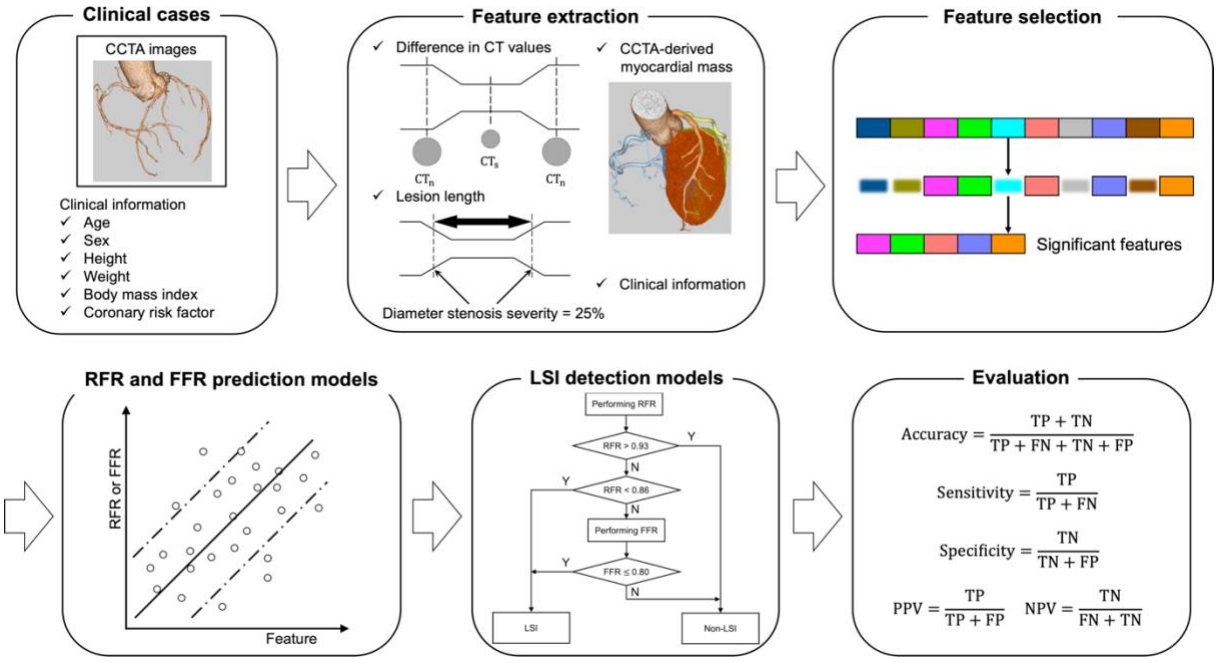

Fig. 3 Scatter plots of the best features selected for the LSI detection models from the (a) RFR ridge prediction model and (b) FFR SVR prediction model. LSI = lesion-specific ischemia, RFR = resting full-cycle ratio, FFR = fractional flow reserve, SVR = support vector regression, DR_{dis} = differential ratio of CT values between non-stenotic and stenotic section in distal lesion, $MMAR_{dis}$ = coronary CT angiography-derived myocardial mass at risk in distal lesion, D_{dis} = difference in CT values between non-stenotic and stenotic section in distal lesion, DR_{prox} = differential ratio of CT values in proximal lesion, L_{prox} = lesion length in proximal lesion.

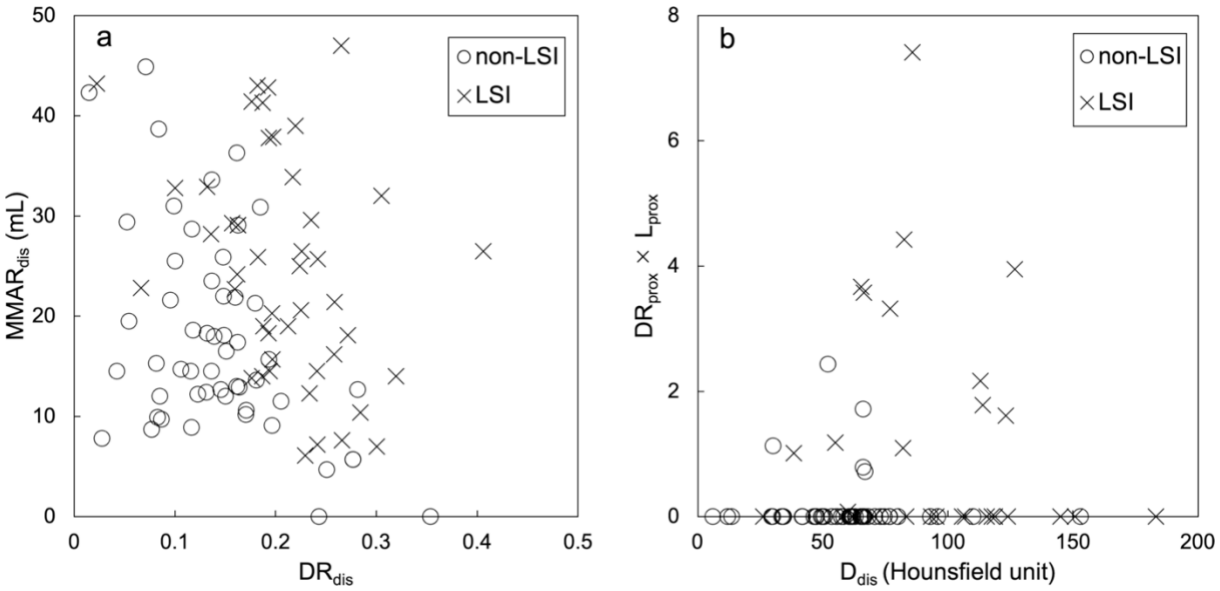

Fig. 4 Two patients with diameter stenosis severity ≥ 50% (white arrow) on CCTA images (a and c). In the first patient (a and b) in a 66-year-old man presenting with chest pain, the LSI detection model with ridge-SVR classified the stenosis in the middle LAD (white arrow) as LSI, with a predicted FFR of 0.75 (a). Invasive coronary angiography also shows the stenosis (white arrow), which was classified as LSI with an invasive FFR of 0.75 (b). In the second patient (c and d) in a 66-year-old man presenting with chest pain, the LSI detection model with ridge-SVR classified the stenosis in the middle LAD (white arrow) as non-LSI, with a predicted FFR of 0.81 (c). Invasive coronary angiography also shows the stenosis (white arrow), which was classified as non-LSI with an invasive FFR of 0.81 (d). CCTA = coronary computed tomography angiography, LSI = lesion-specific ischemia, SVR = support vector regression, LAD = left anterior descending artery, FFR = fractional flow reserve.

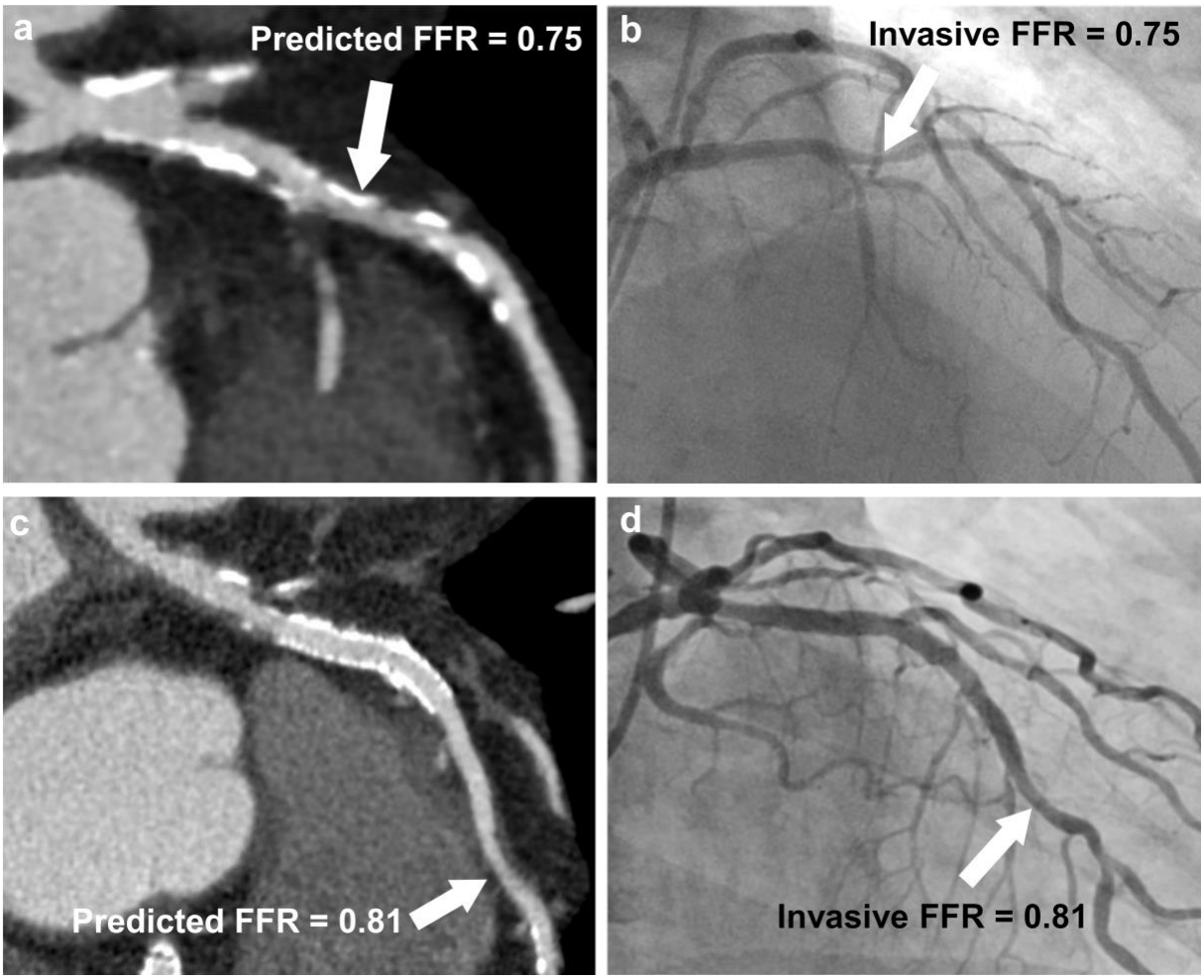

Fig. 5 Evaluation of predicted resting full-cycle ratios (RFRs) using the ridge prediction model. (a) Correlation between invasive and predictive RFRs. (b) Bland-Alman plot of invasive and predicted RFRs.

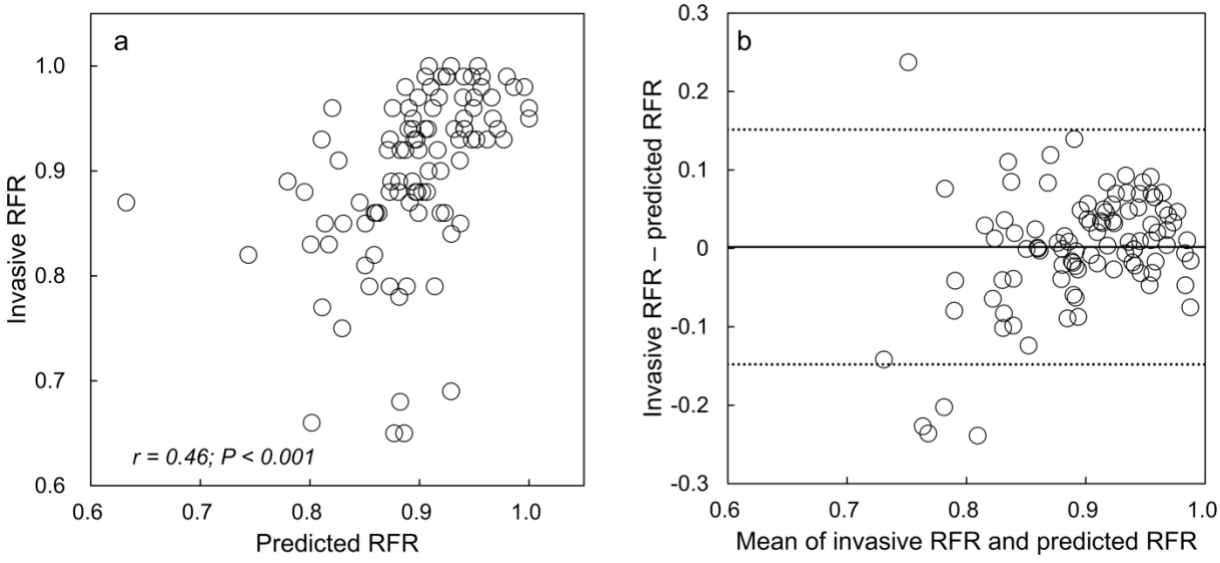

Fig. 6 Evaluation of predicted FFRs using the SVR prediction model. (a) Correlation between invasive and predicted FFRs. (b) Bland-Altman plot between invasive and predicted FFRs. FFR = fractional flow reserve, SVR = support vector regression.

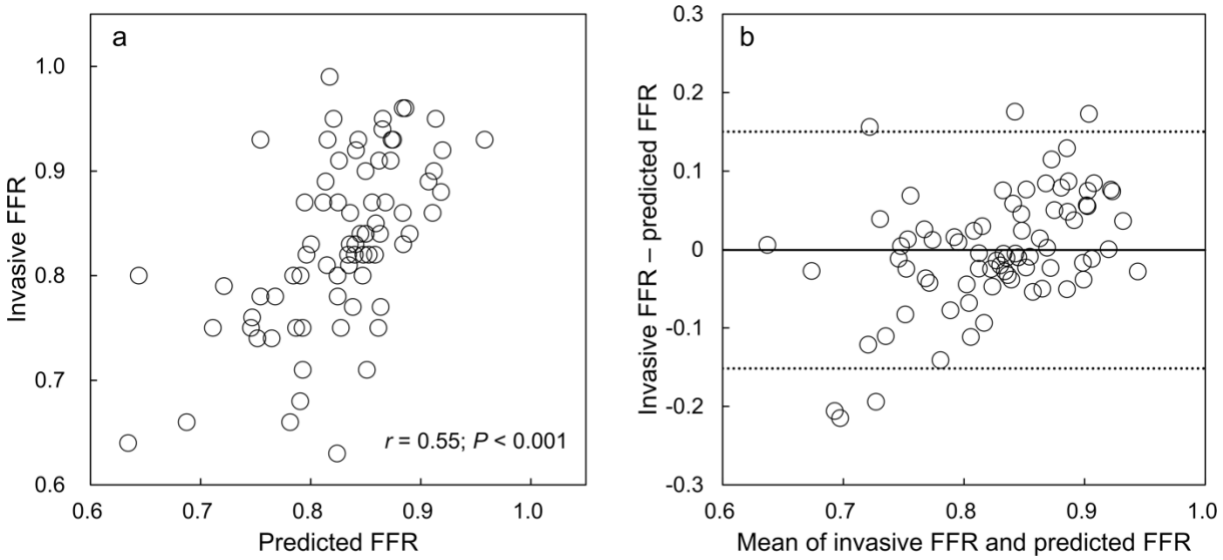

1 **Table**

2 Table 1 Forty-two features used in the prediction models

Coronary computed tomography angiography (CCTA) image	
D_{prox}, Hounsfield units	difference in CT values between non-stenotic† and stenotic section in proximal lesion
D_{dis}, Hounsfield units	difference in CT values between non-stenotic and stenotic section in distal lesion
DR_{prox}	differential ratio of CT values between non-stenotic and stenotic section in proximal lesion
DR_{dis}	differential ratio of CT values between non-stenotic and stenotic section in distal lesion
L_{prox}, mm	lesion length in proximal lesion (≥25% diameter stenosis severity)
L_{dis}, mm	lesion length in distal lesion (≥25% diameter stenosis severity)
DS_{prox}	diameter stenosis severity in proximal lesion
DS_{dis}	diameter stenosis severity in distal lesion
D_{prox}*L_{prox}	product of differences in CT values and lesion length in proximal lesion
D_{dis}*L_{dis}	product of differences in CT values and lesion length in distal lesion
D_{prox}/L_{prox}	ratio of differences in CT values to lesion length in proximal lesion
D_{dis}/L_{dis}	ratio of differences in CT values to lesion length in distal lesion
DR_{prox}*L_{prox}	product of differential ratio in CT values and lesion length in proximal lesion
DR_{dis}*L_{dis}	product of differential ratio in CT values and lesion length in distal lesion
DR_{prox}/L_{prox}	ratio of differential ratio in CT values to lesion length in proximal lesion
DR_{dis}/L_{dis}	ratio of differential ratio in CT values to lesion length in distal lesion
CMM_{total}, mL	CCTA-derived total left ventricular myocardial mass
CMM_{total}/BSA	ratio of the CCTA-derived total left ventricular myocardial mass to BSA
CMM_{major}, mL	CCTA-derived myocardial mass supplied by the major coronary artery containing the lesion
$MMAR_{prox}$, mL	CCTA-derived myocardial mass at risk in the proximal lesion
$MMAR_{dis}$, mL	CCTA-derived myocardial mass at risk in distal lesion
CMM_{major}/CMM_{total}	ratio of the CCTA-derived myocardial volumes supplied by the major coronary artery containing the lesion to the total left ventricular
$MMAR_{prox}/CMM_{total}$	ratio of CCTA-derived myocardial mass at risk in proximal lesion to the total left ventricular

$MMAR_{dis}/CMM_{total}$	ratio of CCTA-derived myocardial mass at risk in distal lesion to the total left ventricular
$MMAR_{prox}/CMM_{major}$	ratio of the CCTA-derived myocardial mass at risk in proximal lesion to the supplied by the major coronary artery containing the lesion
$MMAR_{dis}/CMM_{major}$	ratio of the CCTA-derived myocardial mass at risk in distal lesion to the supplied by the major coronary artery containing the lesion
Valsalva diameter, mm	mean of the long and short diameters in the Valsalva
Clinical information	
Age, years	age
Gender	male or female
Height, m	height
Weight, kg	weight
BMI, kg/m^2	body mass index
BSA, m^2	body surface area
Coronary risk factor	frequency of coronary risk factors
Hypertension	presence or absence of hypertension
Diabetes mellitus	presence or absence of diabetes mellitus
Current smoking	presence or absence of current smoking
Previous PCI	presence or absence of previous PCI
sBP, mmHg	systolic blood pressure
dBP, mmHg	diastolic blood pressure
mBP, mmHg	mean blood pressure
pulse pressure, mmHg	pulse pressure

†Data are mean CT value of the non-stenotic sections proximal and distal to a stenosis.

Table 2 Eighty-eight prediction models comprising combinations of 5 feature-selection methods and 10 regression algorithms

Regression algorithm	Feature selection method
support vector regression (kernel; linear)	RFE, SFFS, SBFS, elastic net, XGB
support vector regression (kernel; radial basis function)†	SFFS, SBFS, elastic net, XGB
least absolute shrinkage and selection operator‡	non, RFE, SFFS, SBFS, elastic net, XGB
ridge	RFE, SFFS, SBFS, elastic net, XGB
elastic net‡	non, RFE, SFFS, SBFS, elastic net, XGB
partial least squares	RFE, SFFS, SBFS, elastic net, XGB
k-nearest neighbor†	SFFS, SBFS, elastic net, XGB
multilayer perceptron‡ (hidden layer size; 6 to 12)	non, SFFS, SBFS, elastic net, XGB
random forest‡	non, RFE, SFFS, SBFS, elastic net, XGB
XGB‡	non, RFE, SFFS, SBFS, elastic net, XGB
light gradient boosting‡	non, RFE, SFFS, SBFS, elastic net, XGB

Note.- XGB = extreme gradient boosting, RFE = recursive feature elimination, SFFS = sequential forward floating selection, SBFS = sequential backward floating selection.

†For regression algorithms that do not assign weights to the features, it is not possible to build the predictive model using RFE.

‡With regression algorithms that allow dimensionality reduction of features, the prediction models were built without using feature selection methods.

1 Table 3 Patient demographics

Variables	LSI cohort (n=40)	Non-LSI cohort (n=36)	P value
Age (year)†	74 ± 12	70 ± 12	0.11
Male sex	26 (65)	25 (69)	0.68
BMI (kg/m^2)†	24.1±3.3	23.7±3.3	0.61
Systolic blood pressure (mm Hg)†	130.1±14.8	130.6±16.8	0.94
Diastolic blood pressure (mm Hg)†	70.6±10.4	73.0±10.1	0.32
Previous percutaneous coronary intervention	12 (30)	18 (50)	0.07
Cardiovascular risk factors			
Hypertension	35 (88)	30 (83)	0.61
Hyperlipidemia	28 (70)	27 (75)	0.63
Current smoking	18 (45)	15 (42)	0.77
Diabetes mellitus	20 (50)	16 (44)	0.63
Target vessel			
Total	46	53	
Left anterior descending artery	32 (70)	23 (43)	< .01
Left circumflex artery	6 (13)	11 (21)	0.31
Right coronary artery	8 (17)	17 (32)	0.09
Other	0 (0)	2 (4)	0.18
Diameter stenosis severity ≥ 50% on CCTA	35 (76)	36 (68)	0.37
Stent implanted	6 (13)	15 (28)	0.06
Fractional flow reserve†	0.74±0.06	0.88±0.05	< .0001
Resting full-cycle ratio†	0.84±0.08	0.95±0.04	< .0001
Therapeutic decision			

Optimal medical therapy	10 (22)	53 (100)	< .0001
Percutaneous coronary intervention	26 (57)	0 (0)	< .0001
Coronary artery bypass grafting	10 (22)	0 (0)	< .0001

Note.- Unless otherwise specified, data are the number of lesions, with percentages in parentheses. BMI = body mass index, CCTA = coronary computed tomography angiography, LSI = lesion-specific ischemia.

†Data are means ± standard deviation.

Table 4 Top 5 features used in the 10 subsets of two LSI detection models

Prediction model	Regression algorithm	#1 feature	#2 feature	#3 feature	#4 feature	#5 feature
Resting full-cycle ratio	Ridge	DR_{dis}	$MMAR_{dis}$	D_{prox}/L_{prox}	DR_{dis}/L_{dis}	DR_{prox}
	PLS	DR_{dis}	$MMAR_{dis}$	D_{dis}/L_{dis}	L_{prox}	D_{dis} *L_{dis}
Fractional flow reserve	SVR	D_{dis}	DR_{prox}*L_{prox}	CMM_{major}	D_{dis}*L_{dis}	D_{prox}*L_{prox}
	Ridge	DR_{dis}/L_{dis}	D_{dis}	DR_{prox}*L_{prox}	D_{dis}/L_{dis}	CMM_{major}

Note.- LSI = lesion-specific ischemia, DR_{dis} = differential ratio of CT values between non-stenotic and stenotic section in distal lesion, D_{dis} = difference in CT values between non-stenotic and stenotic section in distal lesion, L_{dis} = lesion length in distal lesion (≥25% diameter stenosis severity), $MMAR_{dis}$ = coronary CT angiography-derived myocardial mass at risk in distal lesion, DR_{prox} = differential ratio of CT values between non-stenotic and stenotic section in proximal lesion, L_{prox} = lesion length in proximal lesion (≥25% diameter stenosis severity), D_{prox} = difference in CT values between non-stenotic and stenotic section in proximal lesion, CMM_{major} = coronary CT angiography-derived myocardial mass supplied by the major coronary artery containing the lesion.

Table 5 Diagnostic performances for two LSI detection models on vessel and patient basis

RFR regression algorithm (Feature selection method)	Ridge (SBFS)	PLS (SBFS)
FFR regression algorithm (Feature selection method)	SVR linear kernel (Elastic net)	Ridge (SBFS)
Per vessel (n=99)		
Accuracy	0.88 (87/99) [0.81, 0.94]	0.88 (87/99) [0.81, 0.94]
Sensitivity	0.78 (36/46) [0.70, 0.86]	0.83 (38/46) [0.75, 0.90]
Specificity	0.96 (51/53) [0.92, 1.00]	0.92 (49/53) [0.87, 0.98]
PPV	0.95 (36/38) [0.90, 0.99]	0.90 (38/42) [0.85, 0.96]
NPV	0.84 (51/61) [0.76, 0.91]	0.86 (49/57) [0.79, 0.93]
Per patient (n=76)		
Accuracy	0.88 (67/76) [0.81, 0.95]	0.87 (66/76) [0.79, 0.94]
Sensitivity	0.80 (32/40) [0.70, 0.86]	0.85 (34/40) [0.77, 0.93]
Specificity	0.97 (35/36) [0.92, 1.00]	0.89 (32/36) [0.82, 0.96]
PPV	0.97 (32/33) [0.90, 0.99]	0.89 (34/38) [0.83, 0.96]
NPV	0.81 (35/43) [0.76, 0.91]	0.84 (32/38) [0.76, 0.92]

Note.- Data are rate with raw data in parentheses and 95% confidence intervals in brackets.
LSI = lesion-specific ischemia, RFR = resting full-cycle ratio, FFR = fractional flow reserve, PPV = positive predictive value, NPV = negative predictive value, SBFS = sequential backward floating selection, SVR = support vector regression, PLS = partial least squares.

Table 6 Comparisons in diagnostic performance for the detection of lesion-specific ischemia between the present and previous studies

Author (year)	Prediction	No. of patients†	No. of vessels†	Target vessels	Reference	Methods	Sensitivity	Specificity	Accuracy	PPV	NPV
Current study	RFR, FFR	76	99	Intermediate DS	Hybrid RFR-FFR	ML	0.78	0.96	0.88	0.95	0.84
Witberg et al. (2020)	FFR	588	700	Data not available	FFR	RFA	0.91	0.94	0.93	0.91	0.94
Driessen et al. (2019)	FFR	157	505	All	FFR	CFD	0.90	0.86	0.87	0.65	0.96
Coenen et al. (2018)	FFR	351	528	Data not available	FFR	ML	0.81	0.76	0.78	0.70	0.85
Tesche et al. (2018)	FFR	85	107	Intermediate DS	FFR	ML	0.79	0.94	0.87	0.87	0.90

Note.- Unless otherwise specified, data are rate. RFR = resting full-cycle ratio, FFR = fractional flow reserve, DS = diameter-stenosis severity, ML = machine learning, RFA = rapid flow analysis, CFD = computational fluid dynamics, PPV = positive predictive value, NPV = negative predictive value.

†Data are the number.